Green Chemistry

Accepted Manuscript

This article can be cited before page numbers have been issued, to do this please use: S. Clerick, E. De Canck, K. Hendrickx, V. Van Speybroeck and P. Van Der Voort, *Green Chem.*, 2016, DOI: 10.1039/C6GC01494A.

This is an *Accepted Manuscript*, which has been through the Royal Society of Chemistry peer review process and has been accepted for publication.

Accepted Manuscripts are published online shortly after acceptance, before technical editing, formatting and proof reading. Using this free service, authors can make their results available to the community, in citable form, before we publish the edited article. We will replace this *Accepted Manuscript* with the edited and formatted *Advance Article* as soon as it is available.

You can find more information about *Accepted Manuscripts* in the Information for Authors.

Please note that technical editing may introduce minor changes to the text and/or graphics, which may alter content. The journal's standard Terms & Conditions and the Ethical guidelines still apply. In no event shall the Royal Society of Chemistry be held responsible for any errors or omissions in this *Accepted Manuscript* or any consequences arising from the use of any information it contains.

ROYAL SOCIETY OF CHEMISTRY

www.rsc.org/greenchem

View Article Online
DOI: 10.1039/C6GC01494A

Journal Name

ARTICLE

Heterogeneous Ru(III) oxidation catalysts via 'click' bidentate ligands on a Periodic Mesoporous Organosilica support

Received 00th January 20xx,
Accepted 00th January 20xx

DOI: 10.1039/x0xx00000x

www.rsc.org/

Sander Clerick[a], Els De Canck[a], Kevin Hendrickx[a,b], Veronique Van Speybroeck[b] and Pascal Van Der Voort[a]

A 100% monoallyl ring-type Periodic Mesoporous Organosilica (PMO) is prepared as a novel, versatile and exceptionally stable catalytic support with a high internal surface area and 5.0 nm pores. Thiol-ene 'click' chemistry allows straightforward attachment of bifunctional thiols (-NH_2, -OH, -SH) which, exploiting the thioether functionality formed, give rise to 'solid' bidentate ligands. $[Ru(acac)_2(CH_3CN)_2]PF_6$ is attached and complex formation on the solid is studied via Density Functional Theory. All resulting solid catalysts show high activity and selectivity in alcohol oxidation reactions performed in green conditions (25°C/ water). The PMO catalysts do not leach Ru during reaction and are thus easily recuperated and re-used for several runs. Furthermore, oxidation of poorly water-soluble (±)-menthol illustrates the benefits of using hydrophobic PMOs as catalytic supports.

Introduction

The use of selective catalysts and easy recycling thereof, preferably with full recovery, is a major trend in green chemistry. Heterogenization of the active site on a solid support is an elegant method, often explored nowadays, to obtain a catalyst that can be easily separated from the medium by filtration. Herein, it is of paramount importance that the active site does not leach during catalysis. Discovered in 1999, Periodic Mesoporous Organosilicas (PMOs) belong to the most novel and advanced porous silica materials.[1-3] These hybrid silicas are promising support materials as they bear covalently bound organic functionalities (e.g. organocatalysts, ligands) embedded in the pore walls of the silsesquioxane framework, which overcomes leaching issues as compared to classical silanol functionalization methods.[4] Furthermore, PMOs have ordered mesopores, a high degree of hydrophobicity and a high surface area, which contributes to improved mass transfer of organics, hydrolytic stability and the amount of accessible functional groups. Following these properties, the applications of PMOs are not limited to catalysis, as they are also regularly employed in adsorption, controlled drug release, chromatography and as low-*k* materials.[5-7]

In general, PMOs are synthesized by condensation of a silsesquioxane precursor $(RO)_3$-Si-R_f-Si-$(OR)_3$, with OR a hydrolysable group and R_f the bridging organic functionality of interest, around a structure directing template. An extensive amount of R_f-groups have been used, however different synthesis conditions are required as each functionality interacts differently with the reaction medium. Also, larger groups need to be co-condensed or "diluted" with small, non-interacting precursors (e.g. bis(triethoxysilyl)ethane, -benzene) or tetraethylorthosilicate (TEOS) to ensure structural stability. Finally, fixation of R_f in between two Si-framework atoms was described to induce faulty orientation and conformation of the bridged organic functionality, which is especially undesired for bidentate and chiral ligands.[8]

Given its modularity, 'click'-chemistry[9] is a very useful tool for attaching chelating agents via one single covalent bond to a support material, thus allowing free rotation of the ligand. Such covalent attachment is inherently more stable (in water) than conventional but leach-prone grafting of a trialkoxy-organosilane, $(RO)_3SiR_f$, onto free silanol groups of mesoporous silicas (MPS) or PMOs. Moreover, 'click' chemistry yields a more homogeneous distribution of the functionalities within the porous scaffolds, resulting in augmented catalytic activity.[10,11] Specially designed alkyn- or azide organosilicas, either PMOs or MPSs co-condensed with $(RO)_3Si(CH_2)_3N_3$, can easily be transformed by Cu(I) catalyzed azyde-alkyne cycloaddition (CuAAC), into a desired functionality, e.g., dyes, adsorbent moieties or catalysts.[10-14]

Another option is the use of thiol-ene 'click' chemistry[15], which can be performed solely in water at room temperature using an appropriate UV-active radical initiator (as compared to the water/THF mixture used in CuAAC). Thiol-ene chemistry is both readily performed on ethenylene-bridged organosilica precursors in solution[16] as on condensed materials having accessible thiol groups. The latter 'post-modification' was

[a] Department of Inorganic and Physical Chemistry, Ghent University, Krijgslaan 281 S3, 9000 Ghent, Belgium.
[b] Center for Molecular Modeling, Ghent University, Technologiepark 903, 9052 Zwijnaarde, Belgium

Electronic Supplementary Information (ESI) available: NMR characterization of PMO precursors, additional XRD, N_2-sorption and RAMAN experiments, SEM images and computational details. See DOI: 10.1039/x0xx00000x

shown in the attachment of catalytically active chiral quinine, proline or vanadyl-Salen complexes on 3-mercaptopropyl functionalized SBA-15[17-19], in the modification of a thiol bearing PMO with Rose Bengal[20], in organosilane coatings[21] and in the attachment of organosilica nanoparticles on glass.[22] Only recently, our group has modified ethenylene-bridged PMOs[23] by thiol-ene reactions for the first time. Such PMOs, clicked with cysteine and cysteamine, were successfully used in the aldol condensation of 4-nitrobenzaldehyde and acetone.[24]

In 2015, we developed an allyl-functionalized interconnected $[CH_2Si]_3$ ring-type PMO (Fig. 1) with spherical morphology via spray-drying and applied it as a HPLC packing after thiol-ene modification of the allyl groups with a C18-chain.[25] We also showed its exceptional hydrolytic stability (>pH 12 and >150°C), in analogy with similar ring-structured PMOs.[26,27] In order to develop this ultra-stable material into a catalytic support a different synthesis approach is required to improve the pore morphology. Furthermore, the 'dangling' allyl moieties of this material are easily accessible for post-modification. To our knowledge, there are no reports exploiting the thioether functionality inherently created by a thiol-ene 'click' reaction, although the sulphur atom is generally known to interact strongly with late transition metals e.g. Ru, Rh, Pd.

The main focus of alcohol oxidation reactions using ruthenium, either homo- or heterogeneously, lies on the usage of O_2 or air as green oxidants.[28-35] Unfortunately, in almost all reports the reaction is performed at elevated temperatures, in toluene or a halogenated solvent (e.g. trifluorotoluene) and often a co-oxidant is used. High yields are witnessed for aromatic substrates in which the oxidation is driven by expansion of the aromatic system (e.g. oxidation of benzylalcohol to benzaldehyde). Switching to non-aromatic substrates, the yield, however, becomes moderate. Catalytic systems have been described where this Ru-oxidation is performed in water and at room temperature.[36] The trade-off is that periodic acid, H_5IO_6 is used as sacrificial oxidant. However, this cheap, non-toxic oxidant is safe and easy to handle and can be recovered via electrochemistry in a separate process similar to its industrial preparation. In the same report, $[Ru(CH_3CN)_2(acac)_2]PF_6$ is heterogenized on MPS via an NH_2-group and used for the selective oxidation of alcohols. Many substrates are investigated, but leaching and recycling tests are not considered.

Here, we present the hydrothermal synthesis of a novel 100% monoallyl ring-type PMO (mAR) optimized for catalytic applications. The allyl groups are one-step post-modified with reagents of the form HS-$(CH_2)_2$-X, with X = NH_2, OH, SH, to obtain a heterogeneous bidentate ligand in a green and facile manner (Fig. 1). A Ru(III)-complex is anchored onto these chelating ligands inside the PMO pores. The resulting well-defined heterogeneous Ru-catalyst is then tested in the oxidation of carefully selected alcohols in water at room temperature and a recycling and catalyst-leaching assessment is performed.

Experimental

Following chemicals were used as received: 1,1,3,3,5,5-hexaethoxytrisilacyclohexane (HETSCH, 95%, ABCR), tBuLi (1,7M in pentane, Sigma-Aldrich), allylbromide (99%, Sigma-Aldrich), Pluronic P123 (M_n = 5800, Sigma-Aldrich), KCl (≥99.5%, Carl Roth), HCl (37%, Carl Roth), 2-hydroxy-4'-(2-hydroxyethoxy)-2-methylpropiophenone (Irgacure 2959, 98%, Sigma-Aldrich), 2-aminoethanethiol (>95%, TCI Europe), 2-mercaptoethanol (99%, Acros), 1,2-ethanedithiol (≥98%, Sigma-Aldrich), Ruthenium(III)acetylacetonate (99%, STREM), acetonitrile (anhydrous, 99.8%, Sigma-Aldrich), H_2SO_4 (96%, Carl Roth), n-pentane (≥99%, Carl Roth), CH_2Cl_2 (≥99.5%, Carl Roth) toluene (anhydrous, 99.8%, Sigma-Aldrich), ammonium hexafluorophosphate (99%, STREM), H_5IO_6 (99%, ABCR), benzylalcohol (99-100.5%, Sigma-Aldrich), cyclohexanol (99%, Sigma-Aldrich), (±)-menthol (>98%, TCI Europe).

Synthesis of 2-allyl-1,1,3,3,5,5-hexaethoxytrisilacyclohexane (AHETSCH)

In a procedure adapted from Ide et al.[25], 10 ml of HETSCH is dissolved in 30 ml of anhydrous THF under Ar. This solution is heavily stirred at -78.5°C; 1 eq. of t-BuLi is added dropwise over 30 min and the mixture is stirred for another 30 min. By means of a CO_2 cooled syringe, the HETSCH solution is added over 30 min to a separate flask containing 2.2 ml allylbromide (1.07 eq.) in 20 ml of anhydrous THF, cooled to -78.5°C. The reaction is left to stir overnight with temperature gradually increasing to room temperature. The resulting yellow solution is subsequently washed with 25 ml of a 0.2 m% $NaHCO_3$ solution and 2x50 ml of water. Thereafter, the THF-fraction is recuperated and the solvents are evaporated under reduced pressure until a faint yellow oil is obtained (Yield GC: AHETSCH: 52%; HETSCH: 48%; trace impurity of THF adduct). Further purification is performed via column chromatography (silica, hexane:ethylacetate 20:1). Finally, AHETSCH is obtained as a colorless oil.

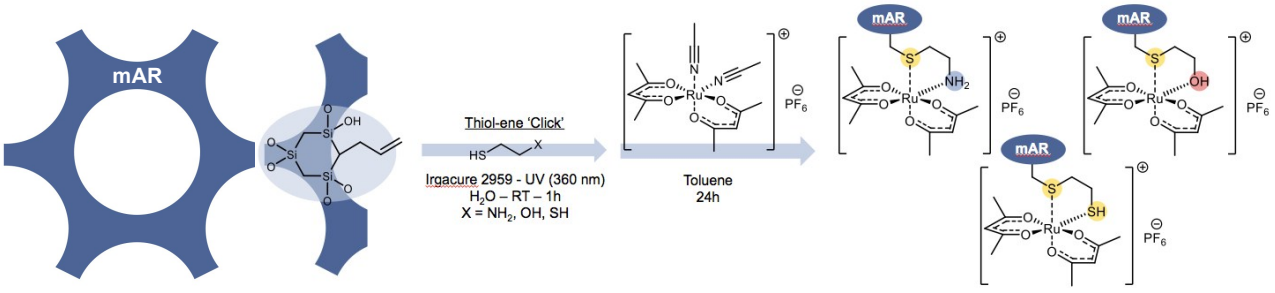

Fig. 1: Schematic representation of the thiol-ene 'click' post-modification and anchoring of $[Ru(acac)_2(CH_3CN)_2]PF_6$ onto the 'solid' bidentate thioether ligands.

^{1}H NMR (300 MHz, $CDCl_3$, Fig. S1) δ = 6.01 (ddt, J=17.0, 9.9, 7.0, 1H, CH2C*H*=CH2), 5.00 (ddd, J=17.0, 3.6, 1.4, 1H, CH=C*H*2), 4.87 (ddt, J=10.0, 2.1, 1.0, 1H, CH=C*H*2), 3.85 – 3.71 (m, 12H, OC*H*2), 2.41 – 2.32 (m, 2H, CHC*H*2CH=CH2), 1.26 – 1.16 (m, 18H, OCH2C*H*3), 0.38 (t, J=6.4, 1H, C*H*(Si)2(CH2CH=CH2)), 0.20 – 0.02(m, 4H, SiC*H*2Si). ^{13}C NMR (400 MHz, $CDCl_3$, Fig. S2) δ = 141.38 (CH2*C*H=CH2), 113.45 (CH=*C*H2), 58.40 - 58.23 - 58.21 - 58.11 (O*C*H2), 28.03 (CH*C*H2CH=CH2), 18.41 - 18.37 (OCH2*C*H3), 14.22 (*C*H(Si)2(CH2CH=CH2)), -1.44 (Si*C*H2Si).

Hydrothermal synthesis of mono-allyl ring-PMO (mAR)

In a 50 ml flask, a mixture is made with molar composition AHETSCH:H_2O:P123:HCl:KCl 1:500:0.0517:8.62:23.5. First, 0.375 g of Pluronic P123 is dissolved in 11.25 ml H_2O. Subsequently, 0.9 ml of HCl (37%) and 2.19 g of KCl is added and the solution is stirred (800 RPM) until a clear blue solution is obtained. Under continued stirring, the reaction mixture is heated to 45°C after which 0.5625 g AHETSCH is added at once. 3 h later, stirring is switched off and the temperature is raised to 95°C in order to promote further condensation of the AHETSCH precursor for 24 h ('ageing' step). A white precipitate is filtered off and washed with 3 x 25 ml H_2O and 3 x 25 ml acetone. The template (P123) is removed during a 6 h Soxhlet extraction in acetone and afterwards, the powder is dried overnight at 120°C under vacuum. The amount of allyl groups is determined gravimetrically by bromination of the double bonds.[37]

'Click' post-modification of mAR to mAR-SX (X = NH_2, OH, SH)

The accessible allyl groups in the pores of mAR react with 2-aminoethanethiol, 2-mercaptoethanol or 1,2-ethanedithiol to obtain solid bidentate ligands, i.e., an amine- (mAR-SNH_2), hydroxyl- (mAR-SOH) or thiol- (mAR-SSH) functionalized thioether, respectively. In a general procedure, 3 eq. of thiol per double bond are mixed with 0.75 eq. of Irgacure 2959 in 20 ml of H_2O and flushed with Ar. 0.5 g of mAR is added and the suspension is stirred at room temperature in a home-made UV reactor (λ = 360 nm) for 1h. The products are filtered as off-white powders and resuspended in H_2O at reflux temperature to remove any leftover reagents. Finally the powders are dried at 110°C for 24 h and loading is determined via CHNS elemental analysis.

Synthesis of $[Ru(acac)_2(CH_3CN)_2]PF_6$ and anchoring onto mAR-SX

As adapted from literature[38], $[Ru(acac)_2(CH_3CN)_2]PF_6$ is prepared by dissolving 1 g of $Ru(acac)_3$ in 100 ml of a 1.5% H_2SO_4 solution in anhydrous acetonitrile and stirring this at room temperature until the red solution turns deep blue (approx. 5 h). Next, 90% of the solution is evaporated and cooled to 0°C. NH_4PF_6 (0.409 g, 1.5 eq.) in 10 ml of H_2O is added under stirring and the solution is left to stand for 30 min. $[Ru(acac)_2(CH_3CN)_2]PF_6$ (85%) is obtained as a blue precipitate which is filtered, washed (2 x 10 ml of ice water, 2 x 10 ml of pentane) and dried for 24 h under vacuum.
Subsequently, $[Ru(acac)_2(CH_3CN)_2]PF_6$ is heterogenized by stirring mAR-SX with 0.5 eq. of complex per bidentate ligand in toluene (100 ml/g mAR-SX) for 24 h at room temperature. The solids (mAR-SX-Ru) are obtained as purple powders after filtration, washing with minimal amounts of CH_2Cl_2 and vacuum drying overnight at 30°C.

Catalytic procedure for the oxidation of alcohols

1 mmol of substrate (benzylalcohol, cyclohexanol, (±)-menthol) is weighed off in a 15 ml reactor; 10 ml of H_2O and the supported catalyst (0.06 mol% Ru) are added, together with 0.1 g of toluene as a standard with similar low solubility as the analytes in water. An extraction efficiency factor is determined for all analytes to compensate for extraction losses. To start the reaction, 1.1 eq. of H_5IO_6 is added while stirring and the reaction is kept at 25°C for 3 h. Then, the solid catalyst is filtered off and the filtrate is extracted 3 times with 25 ml of diethylether. Finally, the samples are analysed by means of gas chromatography. For recycling tests, the catalyst is washed with H_2O and acetone and dried at 30°C overnight. Catalytic profiles are constructed by taking 1 ml aliquots at set times. To test the heterogeneity of the catalyst, the solid is filtered off (0.45 μm membrane) after 10 min of reaction time and the catalytic activity of the filtrate is further evaluated (hot filtration test).

Characterization and analysis

^{1}H NMR spectra of AHETSCH are recorded in $CDCl_3$ on a Bruker 300 MHz AVANCE spectrometer with chemical shifts (δ) expressed in ppm relative to a tetramethylsilane standard. ^{13}C NMR was performed on a Bruker Avance III 400 MHz spectrometer. X-ray powder diffraction (XRPD) patterns of all mAR-PMOs are recorded on a Thermo Scientific ARL X'TRA X-ray diffractometer using Cu Kα radiation of 40 kV and 30 mA. A Micromeretics Tristar II is used for N_2-sorption experiments at 77 K to obtain the internal surface area (S_{BET}) and pore size distribution ($d_{p,BJH}$) making use of the BET and BJH theory, respectively. Diffuse Reflectance Infrared Fourier Transform Spectroscopy (DRIFTS) is performed using a Thermo Nicolett 6700 FT-IR spectrometer equipped with a Greasby-Specac diffuse reflectance cell, modified to measure samples at 20 – 300°C under vacuum. For CHNS elemental analysis, a Thermo Flash 200 elemental analyser is used with V_2O_5 as catalyst. Transmission electron microscopy (TEM) images are taken on a JEOL JEM 2200-FS TEM and scanning electron microscopy (SEM) images on a JEOL JSM 7600F FEG SEM. Ru loadings (Kα) are determined by X-ray fluorescence (XRF) on a Rigaku NEX CG with an Al source and compared to Sr-Kα as internal standard. All catalytic tests are analyzed with an ultrafast TRACE GC (Thermo, Interscience) equipped with a flame ionisation detector and a 5% diphenyl / 95% poly-dimethylsiloxane column (10 m x 0.10 mm) using He as carrier gas at 0.8 mL/min.

Computational Methodology

All calculations are performed within the Gaussian09 (G09) package[39] using Density Functional Theory (DFT). Calculations are performed using the B3LYP[40,41] and OPBE[42-45] functionals and a Def2-TZVP polarized split-valence triple-ζ basis set.[46,47] Dispersion corrections are added using Grimme's DFT-D3

version[48] with Becke-Johnson damping.[49] The coefficients for the OPBE calculations are taken from Goerigk et al.[50] (S8 = 3.3816, a1 = 0.5512 and a2 = 2.9444) and defined manually in the Gaussian program. Furthermore, a correction energy for the Basis Set Superposition Error (BSSE) is calculated using the Boys and Bernardi Counterpoise correction.[51]

Results and Discussion

mAR-PMO as a stable and multifunctional catalytic support

The synthesis and work-up of AHETSCH as the PMO-precursor is successfully optimized, yielding a pure compound and no longer a mixture of mono-, bis- and trisallylated HETSCH (Fig. S3) as described before.[25] The importance of this purification is seen in the X-Ray diffractograms (Fig. 2) of mAR and a PMO, denoted mixAR, synthesized in the same conditions as mAR but using the unpurified precursor mixture. For mAR, an intense (100) reflection peak is distinguished, together with less intense second order (110) and (200) peaks, which are indicative for the 2D hexagonal (*P6mm*) ordered pore structure of the material. The diffractogram of mixAR is however lacking the second order peaks, indicating the loss of long-range ordering. These results are clearly confirmed in the TEM images of both materials (Fig. 2) where ordering is found throughout the entire rod-shaped mAR particles (SEM image: Fig. S4). The mixAR-PMO only shows patches of ordered pores with variable alignment. The major enhancement of pore ordering for mAR is ascribed to a more uniform rate of hydrolysis and condensation of purified AHETSCH. Approximately the same unit cell parameter (a_0) for mAR is seen in the images as calculated via XRD (Table 1).

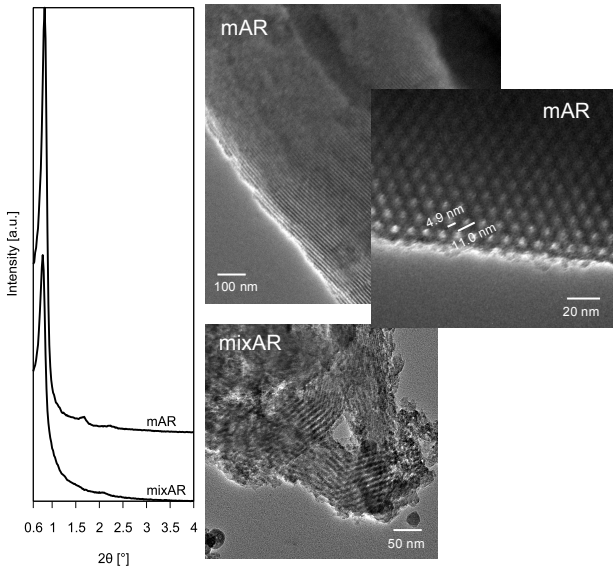

Fig. 2: XRD diffractograms of the 100% monoallyl PMO (mAR, top) and the mixed precursor PMO (mixAR, bottom). TEM images confirm the ordered pore geometry of mAR.

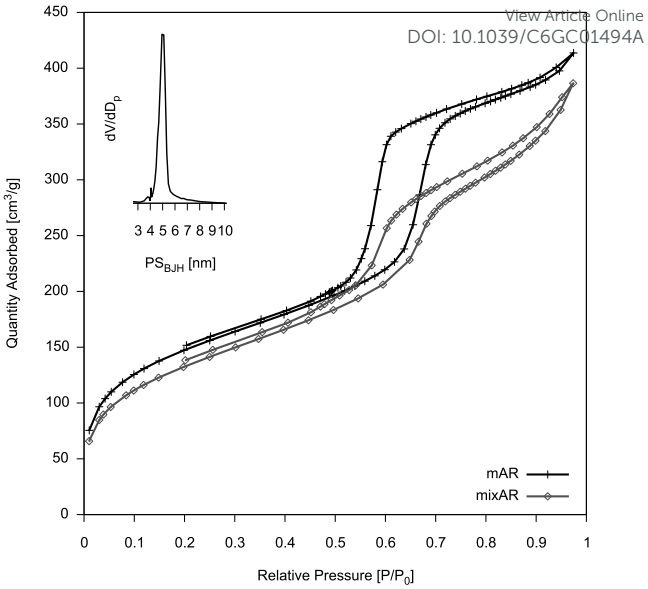

Fig. 3: N_2-sorption isotherms of mAR and mixAR. Inset: BJH pore size distribution plot of mAR.

In terms of porosity similar differences are also observed. N_2-sorption experiments (Fig. 3) show type IV isotherms with sharp H1 hysteresis for mAR, typical for highly ordered mesoporous materials with uniform cylindrical pores (SBA-15 like). mAR shows a high internal surface area (S_{BET} = 536 m^2/g) with 5.0 nm pores ($d_{p,BJH}$) in accordance with TEM images. Comparable results are obtained for mixAR (S_{BET} = 472 m^2/g, $d_{p,BJH}$ = 5.1 nm) but the pore size distribution is broadened and increased macroporosity, attributed to irregular, disordered areas, is witnessed. Given that the slightest disorder of mesopores already has a significant impact on the diffusion of molecules within these pores[52], results of this structural assessment clearly indicate the superior quality of mAR as a catalytic support.

Furthermore, we have tested the hydrolytic stability of mAR-PMOs by stirring the material in a 1M HCl solution and a 0.1M NaOH solution at room temperature. XRD and N_2 sorption (Fig. S5, Table S1) show no structural change for the acid treated samples. Also, the material remains unaffected after 3h in strong basic medium. Only after 24h at pH 13 mAR starts to show the first signs of deterioration, indicated by a small drop in surface area and pore size. This exceptional hydrolytic stability compared to other silicas makes mAR highly suitable

Table 1: Structural properties of the synthesized PMO materials.

	mAR	mAR-SNH_2	mAR-SNH_2-Ru	mAR-SOH	mAR-SOH-Ru	mAR-SSH	mAR-SSH-Ru
S_{BET} [a] (m^2/g)	536	400	271	343	309	304	208
V_p [b] (ml/g)	0.48	0.45	0.32	0.44	0.39	0.46	0.28
$d_{p,BJH}$ [c] (nm)	5.0	5.1	4.8	5.0	5.0	5.1	5.1
a_0 [d] (nm)	12.1	12.1	12.0	12.0	11.9	11.9	11.8

[a] Specific surface area determined via Brunauer-Emmett-Teller theory. [b] Pore volume determined from adsorption branch at P/P_O = 0.99. [c] Pore size calculated from desorption branch following Barrett-Joyner-Halenda theory. [d] XRD unit cell parameter ($a_0 = 2d_{100}/\sqrt{3}$) for P6mm 2D hexagonal ordering.

for reactions requiring extreme pH in water. The hydrophobicity of mAR not only explains its stability as we experienced before[25,26], but might also enhance mass transport of organics towards the catalytic support in water (see catalytic tests).

'Click' post-modification of the allyl functional handles

The allyl groups of mAR are readily transformed into any organic functionality of interest via thiol-ene 'click' chemistry. The amount of accessible double bonds is gravimetrically estimated at 2.4 mmol/g by performing a gas-phase bromination reaction. The functional loading of the resulting materials (CHNS) after 'click' reaction with 2-aminoethanethiol (mAR-SNH_2), 2-mercaptoethanol (mAR-SOH) and 1,2-ethanedithiol (mAR-SSH, after reduction of possible disulfide bridges) on mAR is found in Table 2. Treatment of 1h in the UV reactor already leads to high functional loading (ca. 1.7 mmol/g) for mAR-SOH and mAR-SSH. No further increase of functionality is observed for a reaction time of 3h or even 24h. The 'click' reaction of 2-aminoethanethiol is shown to be less

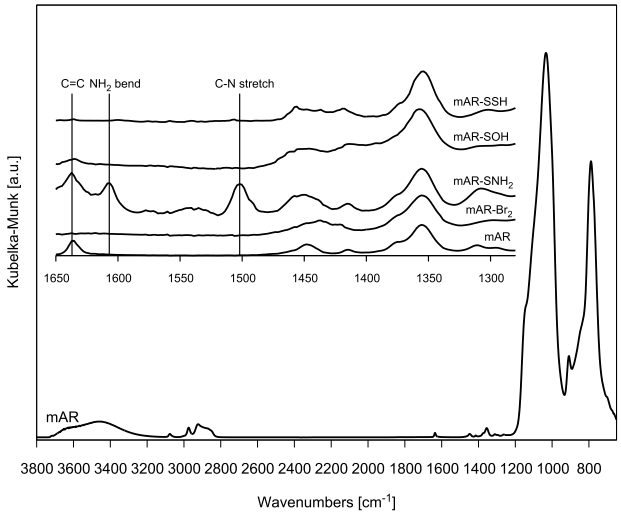

Fig. 4: DRIFT spectrum of mAR. Inset: Zoom of the region of interest for reaction on the allyl groups.

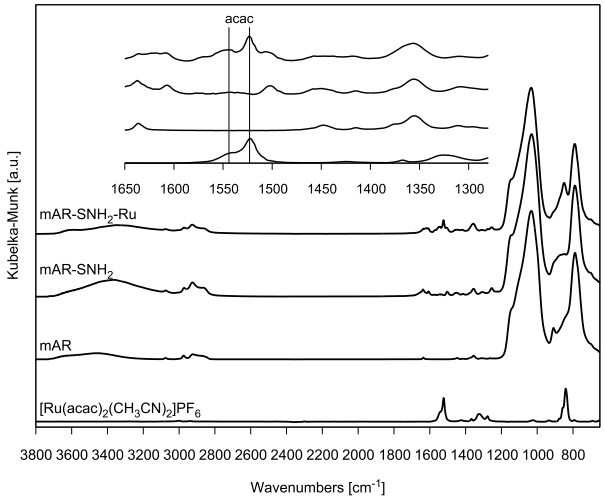

Fig. 5: DRIFT spectrum of the homogeneous $[Ru(acac)_2(CH_3CN)_2]PF_6$ complex, mAR, mAR-SNH_2 and mAR-SNH_2-Ru.

Table 2: Functional loading after 'click' post-modification and Ru anchoring.

	mAR-SNH_2-Ru	mAR-SOH-Ru	mAR-SSH-Ru
Lig.[a] (mmol/g)	0.73	1.70	1.72
Ru[b] (mmol/g)	0.204	0.049	0.040
%[c]	27	2.9	2.3

[a] Ligand loading determined from S-content in CHNS elemental analysis. [b] Ru loading determined via XRF. [c] Amount of ligands functionalized with Ru(III).

effective (0.73 mmol/g). For all post-modification steps, a drop in S_{BET} is observed as a result of the mass increase of the material and the decoration of the pore walls with the functionalities (Table 1). Furthermore, no structural degradation is observed in the XRD diffractograms after functionalization. (Fig. S6)

The infrared spectrum (DRIFTS) of mAR is given in Fig. 4. Next to C-H and 2 Si-O-Si stretch vibrations, in the region 2950-2800 cm^{-1}, 1200-1000 cm^{-1} and 800 cm^{-1}, respectively. Distinct peaks show up at 3070, 1640 and 890 cm^{-1} testimonial for the allyl-groups (olefin C-H stretch, C=C stretch and olefin C-H out of plane deformation). Vibrations in the 1475-1280 cm^{-1} region are typical for the modified ring structure. After bromination reaction (mAR-Br_2), it is clear that all C=C vibrations (1640 cm^{-1}) have disappeared (Fig. 4, zoom), implying that Br_2 gas, due to its small size, reacts with allyl groups in the micropores and/or penetrates inside the pore walls. This makes us believe that the gas-phase bromination reaction overestimates the amount of reachable double bonds inside the material. During the functionalization process in water, the thiols cannot reach all of these allyl groups, indictated by the persisting C=C peaks in the IR spectrum. In accordance with a lower loading (CHNS), a less drastic decrease is observed for mAR-SNH_2, however, the primary amine gives rise to the appearance of new vibration peaks at 1607 and 1502 cm^{-1} (NH_2 bend and C-N stretch). O-H stretches (mAR-SOH) are not observed due to overlap with residual adsorbed water. S-H vibrations (mAR-SSH) are distinguished at 2570 cm^{-1} in the RAMAN spectrum (Fig. S7).

Table 2 also shows the amount of $[Ru(acac)_2(CH_3CN)_2]PF_6$ anchored onto the bidentate ligands created on the PMO. In mAR-SNH_2, Ru is attached to up to 27% of the SNH_2 ligands. In DRIFTS, the characteristic peaks of $[Ru(acac)_2(CH_3CN)_2]PF_6$, e.g. acac carbonyl stretches at 1544 and 1523 cm^{-1}, are superimposed on the mAR-SNH_2 spectrum to form mAR-SNH_2-Ru (Fig. 5). Given the meticulous washing step, this indicates that anchoring of the Ru-complex is successful. As a 10 fold less Ru gets anchored to the SOH and SSH ligands, the Ru-complex peaks can no longer be identified. After anchoring, the PF_6 counter ion remains present as confirmed by XRF.

Unfortunately, DRIFTS does not provide sufficient evidence of the exact complex formation once the Ru-complex is heterogenized. Furthermore, other techniques (e.g. XPS) proved insufficient because of the low Ru loading compared to the PMO matrix. Therefore, we conducted a computational study on a simplified ligand—Ru(III) model to explain the nature of complex formation.

Computational study of complex formation

View Article Online
DOI: 10.1039/C6GC01494A

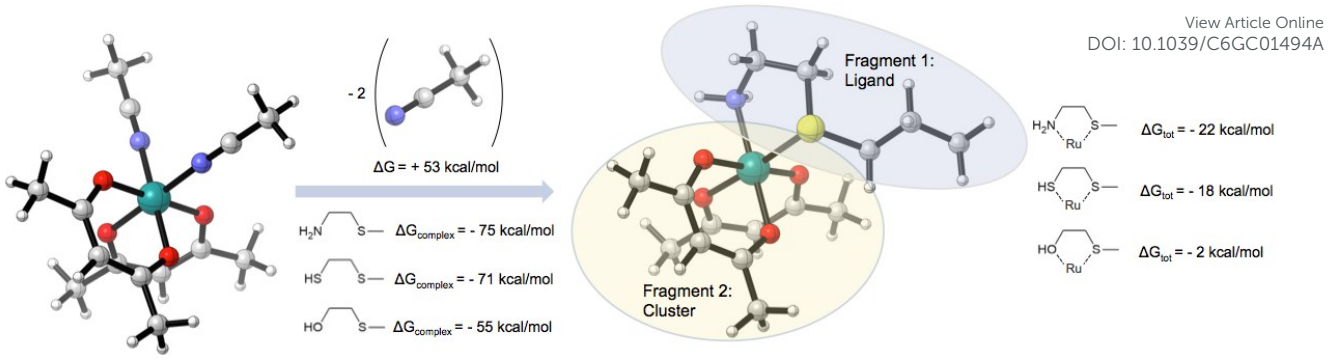

Fig. 6: Computational model with two fragments indicated. Total charge of the system is +1 and it has a doublet spin state

To study the complexation process of the Ru catalyst to the PMO anchored ligands, a simplified model system is constructed (Fig. 6). This model comprises the Ru centre, surrounded by two acac groups and the ligand of interest, terminated by a methyl group. We assume that the large pore diameter of 5 nm gives a large curvature and hence limited interactions with the pore wall are expected. Therefore, the PMO environment is neglected during the calculations.[24] This simple model system allows us to investigate whether the complexation to the ligand is thermodynamically favoured, compared to the original $[Ru(acac)_2(CH_3CN)_2]^+$ complex, and hence corroborate that the complex is anchored to the PMO.

Open shell transition metal systems are notoriously difficult for DFT methods to predict correct spin states and geometries. Recent studies have shown that the OPBE functional performs very well for transition metal complexes.[53,54] For comparison, B3LYP calculations are also performed, since this widely tested functional still proves to be very robust for organic systems.[55] More details on the computational method can be found in SI. Both functionals gave the same qualitative understanding of the system and predict complexation energies that are in the same range. The calculations (Fig. 6 and Table S2) show that the bidentate linkers can effectively bind the complex with large interaction strength for every type of ligand.

In conclusion, theoretical calculations support that the complex formation with the bidentate ligand is thermodynamically favourable compared to the starting complex. Furthermore, the amine ligand has the strongest interaction with the Ru complex, which supports the higher Ru loading of mAR-SNH_2-Ru. In order to have a more physically correct point of view, we compared the anchored ruthenium to the original complex as a reference system, which is schematically represented in Fig. 6. Here, we first calculate the energy cost to 'remove' both acetonitrile groups and the consecutive stabilization caused by the recomplexation to the new ligand, representative for the actual experimental exchange process. Using this approach, we find that the anchoring to the new ligand is thermodynamically favoured by 2 - 22 kcal/mol depending on the ligand (an order of NH2 > SH > OH is found).

Catalytic alcohol oxidation in water

For catalytic tests, we retained three different materials: mAR-SOH-Ru, mAR-SSH-Ru with relatively low Ru loading and mAR-NH_2-Ru with a relatively high Ru loading. Although the pore walls of these PMOs are relatively hydrophobic, all catalysts are homogeneously dispersed in water courtesy of the remaining silanol groups. In our initial experiments, we performed the oxidation of benzylalcohol, as this is the substrate of choice in many reports on Ru catalyzed oxidation reactions[35-36]. However, in our system, we already observe full conversion of benzylalcohol to benzaldehyde without addition of a Ru-catalyst (blank reaction). We assume that benzylalcohol and similar substrates are easily oxidized as expansion of the π-system pushes the reaction towards full conversion.

Therefore, we selected cyclohexanol as non-aromatic substrate, which does not benefit from conjugation after oxidation. Catalytic results are represented in Table 3. All considered Ru-catalysts show full conversion of cyclohexanol after 180 min, whereas for the blank reaction only 12% is observed. This reaction is roughly four times faster compared to $[Ru(acac)_2(CH_3CN)_2]PF_6$ anchored on an aminopropyl grafted silica[36], which nicely illustrates the enhanced diffusion of organics in water towards the hydrophobic PMO materials. The results, however, show a discrepancy between $[Ru(acac)_2(CH_3CN)_2]PF_6$ and the solid PMO catalysts in terms of selectivity. A similar loss in selectivity is seen if homogeneous $Ru(acac)_3$ is used as catalyst. Here, a vacant reaction site must be created by the expulsion of an acac-ligand, which causes a tendency for overoxidation (by-products were determined as cyclohexenone and hydroquinone). Overreaction does not occur when the weakly bound CH_3CN ligands of $[Ru(acac)_2(CH_3CN)_2]PF_6$ are removed. This fact thus suggests

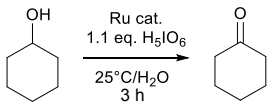

Table 3: Oxidation of cyclohexanol

Entry	Catalyst	Ru (mol%)	Conv.[a] (%)	Yield[a] (%)
1	$[Ru(acac)_2(CH_3CN)_2]PF_6$	5	>99	>99
2	$Ru(acac)_3$	2.5	93	88
3	mAR-SNH_2-Ru	0.06	>99	95
4	mAR-SOH-Ru		>99	81
5	mAR-SSH-Ru		>99	80
6	Blank	0	12	12

[a]GC-determined with toluene as internal standard

that Ru is indeed anchored to mAR-SX by exchange of the weak acetonitrile ligands corroborating with the assumption made in the computational study.

Next, we constructed reaction profiles for mAR-SOH-Ru, mAR-SSH-Ru and mAR-SNH_2-Ru and performed 'hot-filtration' tests (Fig. 7) to determine whether the catalysis takes place exclusively on the PMO surface. Given the reaction profiles of mAR-SOH-Ru and mAR-SSH-Ru, the optimum reaction time is 40 min with a high TOF_{10min} of 1.53 s^{-1} and 1.47 s^{-1}, respectively. At this optimum, all cyclohexanol is selectively oxidized into cyclohexanone and only thereafter further oxidation products are formed as a result of continuing β-elimination reactions.[56] The dashed line in Fig. 7 shows the reaction profile during the hot filtration (HF) test. For both materials, separation of the catalyst from the reaction mixture occurred after 10 min. No further reaction is witnessed in the filtrates but the blank reaction. This, combined with the fact that no leaching of Ru was observed in the filtrate at ppm level (XRF) shows that the reaction occurs on the pore surface of the PMO and that we have developed non-leaching, fully heterogeneous and recyclable catalysts. The latter statement is demonstrated in Fig. 8, where catalyst-recycling experiments for mAR-SOH-Ru show a similar activity for 3 consecutive catalytic runs of 180 min, without loss of structural ordering of the support (Fig. S8). The total reactant conversion is similar for all runs. However, as seen in the reaction profiles, the occurring reaction is sequential (-ol → -one → enone/hydroquinone). Therefore, the lower yield of cyclohexanone in Run 1 and 3 is accompanied by an increase of the overoxidation products. We believe that this slight variability in the yield of cyclohexanone is due to small changes in the kinetics of the reaction that could be caused by external factors.

However, when immersing mAR-SNH_2-Ru in the reaction medium and filtering off the catalyst after 10 min, we observed further reaction in the filtrate. The conversion of cyclohexanol in the filtrate increased from 35% at the time of filtration to 83%, significantly more than expected for the blank reaction. This indicates that the Ru-complex is detached from the support and partially leaches into the medium, where it can no longer be recovered. Via XRF, the Ru-leaching is determined at 30% after 3 catalytic runs. To ensure this leaching is not loading related, we prepared a mAR-SNH_2-Ru sample for which the anchoring was executed in acetone, to obtain a catalyst with similar Ru-loading (0.037 mmol/g) to mAR-SOH-Ru and mAR-SSH-Ru. Again, the hot filtration test was unsuccessful. The very different behaviour of mAR-SNH_2-Ru can be explained by taking into account the reaction medium. H_5IO_6 not only acts as the oxidant, it can also readily protonate the NH_2-group of the ligand, whereas –OH and –SH remain unaltered.

This is confirmed in our computational study. The acidic environment created by the periodic acid (pKa 3.29) is sufficiently strong to protonate the amine group of the ligand (approx. pKa 10). This leads to a subsequent change in the conformation of the complex as is shown in Fig. 9. The now positively charged amine group turns away from the Ru centre, and only a weak interaction of the sulphur lone pair (about 6 kcal/mol) remains, not sufficient to retain the complex in that position.

The hydroxyl group (approx. pKa -2) and the thiol group (approx. pKa -7) of the other ligand chains cannot be protonated in this reaction environment and therefore stay in the same conformation. These results explain why ruthenium leaching is only observed for the amine-based ligand, notwithstanding that this ligand has the strongest affinity to bind the ruthenium complex.

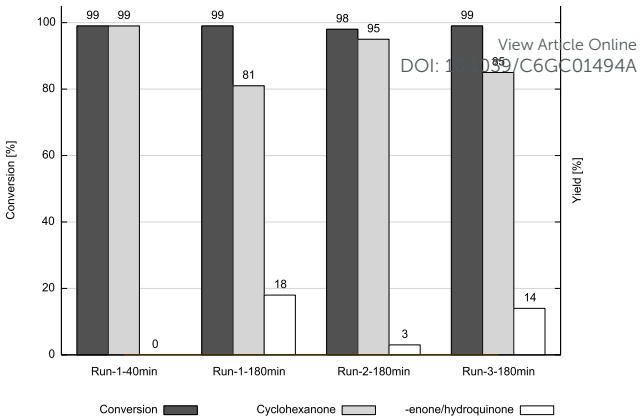

Fig. 8: Catalyst recycling experiment for mAR-SOH-Ru, with conversion of cycyclohexanol (dark grey), yield of cyclohexanone (grey) and formation of the byproducts, cyclohexenone and hydroquinone (white)

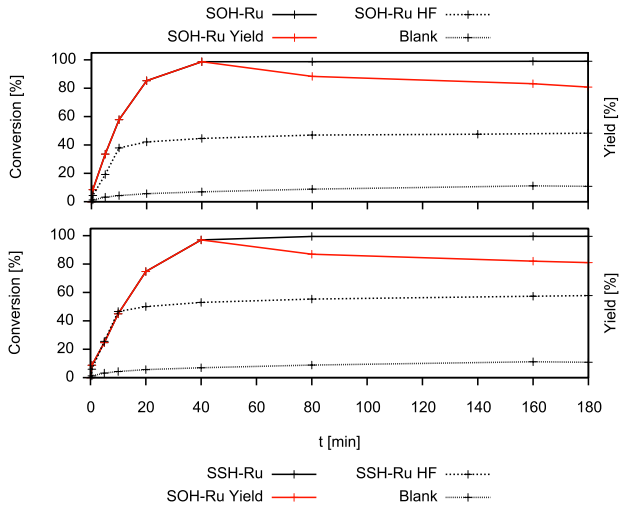

Fig. 7: Reaction profiles of mAR-SOH-Ru (top) and mAR-SSH-Ru (bottom). A hot filtration test (HF) is performed with filtration at t = 10 min (dashed).

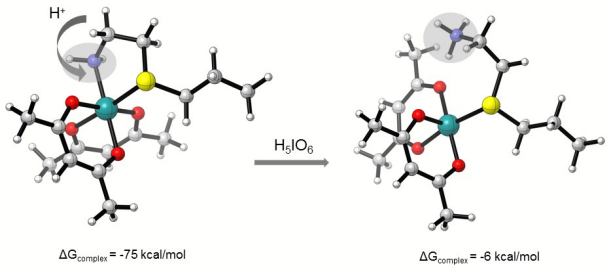

Fig. 9: In an acidic environment, the amine group can be easily protonated. The remaining S—Ru interaction is rather weak and as a consequence, the complex leaches out.

As a control experiment, we prepared an aminopropyl grafted SBA-15 and subsequently anchored $[Ru(acac)_2(CH_3CN)_2]PF_6$ (details in SI). For this catalyst, the Ru is no more stabilized by the sulphur atom after protonation of the amine group. Here, up to 50% of Ru is leached after 1 catalytic run, whereas for mAR-SNH_2-Ru 30% of Ru leaching is observed after 3 runs. These results prove that the amine group indeed causes leaching by protonation in the acidic medium. Also, the small stabilizing effect of the lone sulphur atom is witnessed given the less pronounced leaching for mAR-SNH_2-Ru.

Mechanistic insights

In Fig. 10, a mechanism for this catalytic oxidation is proposed. In our system at 25°C, the acidity of H_5IO_6 is needed to expel an acac-ligand and to create vacant Ru-sites as indicated by the catalytic activity of $Ru(acac)_3$. Furthermore, we did not observe conversion if $NaIO_4$ is used as neutral oxidant at room temperature, demonstrating that the acidity is decisive for catalytic activity. It is generally accepted that alcohols undergo β-elimination in the presence of late transition metals, which is often regarded as the rate-determining step.[28,30,57,58] Here, the resulting Ru-H_2 is readily oxidized by the periodate anion. Although the latter is consumed during reaction, electrochemical regeneration is straightforward. By-products of the cyclohexanol oxidation, cyclohexenone and hydroquinone, are the result of extended β-elimination. This side-reaction is far less favourable as these products are only formed after full conversion to cyclohexanone. We believe the selectivity of the reaction arises from selective coordination of cyclohexanol to vacant Ru sites followed by ß-elimination. Given the reaction profile, cyclohexanone, the reaction product, must only be able to coordinate to the vacant sites after all cyclohexanol is consumed to yield cyclohexenone.

Finally, we attempted cyclohexanol oxidation with either H_2O_2 or O_2 as the oxidant at low pH to promote the removal of the acac group. No conversion of the substrate was observed after 180 min. This results from the lower oxidation potential of H_2O_2 and O_2 compared to H_5IO_6, which is insufficient to regenerate the active Ru(III)-species.

Arguably, in all performed catalytic reactions, H_5IO_6 is used as a sacrificial oxidant. However, after filtration of the Ru catalysts and subsequent extraction of the reaction products, only an aqueous phase containing HIO_3 remains. In potential applications, this latter can be reconverted into a H_5IO_6 solution within the same medium via an electrochemical procedure in a separate cycle. This, combined with the catalyst recycling, the use of water as a solvent and performing the reaction at room temperature, provides a sustainable alternative to current aerobic oxidation reactions at elevated temperature in organic solvents.

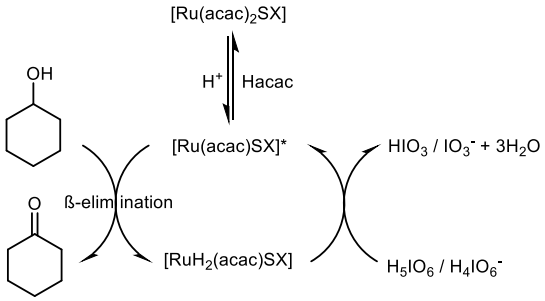

Fig. 10: Schematic mechanism of H_5IO_6 heterogeneous cyclohexanol oxidation. X = OH, SH coming from mAR.

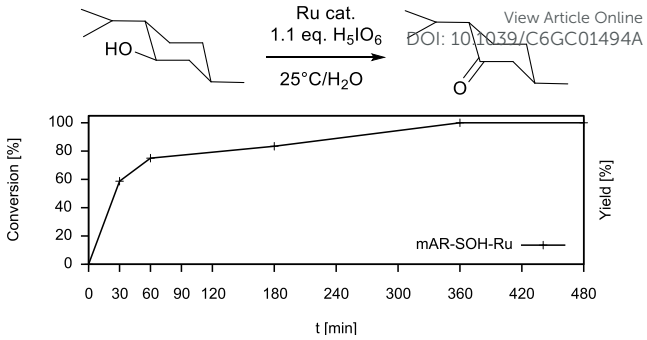

Fig. 11: Reaction profile for (±)menthol oxidation with mAR-SOH-Ru as catalyst.

Oxidation of poorly water-soluble alcohols

As a final experiment, we selected (±)-menthol as a sterically hindered, poorly water-soluble substrate. Such substrates are notoriously hard to oxidize in water/RT and no selective, complete conversion is reported even after reaction for >12h.[31,36] Albeit the poor solubility of (±)-menthol in water, we obtain full conversion after 6 hours, with >99% selectivity towards menthone with our PMO catalyst (mAR-SOH-Ru) (Fig. 11). This remarkable behaviour must be attributed to the properties of the mAR-PMO support. Sequential hydrophobic/hydrophilic 'zones' in the PMO material, originating from the organic bridges and siloxane/silanol functionalities, create an ideal reaction environment for the reaction of hydrophobic molecules in water.[24, 59-63] Therefore, reactants are locally enriched and/or reaction products are repelled which, combined with an ordered pore structure, results in high catalytic activity (TOF_{30min} = 0.54 s^{-1}). No further β-elimination products are found, which implies that steric hindrance of the isopropyl and methyl groups prevent overreaction.

Conclusion

We have developed a novel and exceptionally stable 100% monoallyl ring-type PMO (mAR) of which structure and porosity (536 cm^2/g, 5.0 nm pores) are optimized to serve as a catalytic support material. Via thiol-ene 'click' chemistry, the allyl groups protruding in the pores are transformed into three distinct bidentate thioether ligands (SNH_2, SOH, SSH). Experiments and theoretical calculations confirm the heterogenization of a Ru(III)-complex onto these solid ligands. Although protonation of the amine group in the acidic catalytic medium causes leaching for mAR-SNH_2-Ru, mAR-SOH-Ru and mAR-SSH-Ru are successfully applied as selective, truly heterogeneous catalysts in the oxidation of cyclohexanol in water at 25°C. Moreover, the hydrophobic/hydrophilic reaction environment and ordered pores of the mAR-support

enable high catalytic activity for a poorly water-soluble and sterically very challenging substrate such as (±)-menthol.

Acknowledgements

The authors would like to thank T. Planckaert for CHNS elemental analysis and K. Haustraete for TEM imaging. The Research Board of Ghent University (BOF, UGent GOA Grant 01G00710), and the European Research Council (FP7(2007-2013) Grant Agreement 240483) are acknowledged for their financial support. Computational resources and services were provided by the Stevin Supercomputer Infrastructure of Ghent University and by the Flemish Supercomputer Center (VSC), funded by the Hercules Foundation and the Flemish Government-Department EWI.

Notes and references

1 T. Asefa, M. J. MacLachlan, N. Coombs and G. A. Ozin, *Nature*, 1999, **402**, 867-871.
2 S. Inagaki, S. Guan, Y. Fukushima, T. Ohsuna and O. Terasaki, *J. Am. Chem. Soc.*, 1999, **121**, 9611-9614.
3 B. J. Melde, B. T. Holland, C. F. Blanford and A. Stein, *Chem. Mater.*, 1999, **11**, 3302-3308.
4 M. Ferre, R. Pleixats, M. W. C. Man and X. Cattoen, *Green Chem.*, 2016, **18**, 881-922.
5 P. Van der Voort, D. Esquivel, E. De Canck, F. Goethals, I. Van Driessche and F. J. Romero-Salguero, *Chem. Soc. Rev.*, 2013, **42**, 3913-3955.
6 N. Mizoshita, T. Tani and S. Inagaki, *Chem. Soc. Rev.*, 2011, **40**, 789-800.
7 F. Hoffmann, M. Cornelius, J. Morell and M. Froeba, *Angew. Chem., Int. Ed.*, 2006, **45**, 3216-3251.
8 C. Baleizao, B. Gigante, D. Das, M. Alvaro, H. Garcia and A. Corma, *Chem. Comm.*, 2003, 1860-1861.
9 H. C. Kolb, M. G. Finn and K. B. Sharpless, *Angew. Chem., Int. Ed.*, 2001, **40**, 2004-2021.
10 J. Nakazawa, B. J. Smith and T. D. P. Stack, *J. Am. Chem. Soc.*, 2012, **134**, 2750-2759.
11 J. Y. Shi, C. A. Wang, Z. J. Li, Q. Wang, Y. Zhang and W. Wang, *Chem.-Eur. J.*, 2011, **17**, 6206-6213.
12 K. Buerglova, A. Noureddine, J. Hodacova, G. Toquer, X. Cattoen and M. W. C. Man, *Chem.-Eur. J.*, 2014, **20**, 10371-10382.
13 A. Schachtschneider, M. Wessig, M. Spitzbarth, A. Donner, C. Fischer, M. Drescher and S. Polarz, *Angew. Chem., Int. Ed.*, 2015, **54**, 10465-10469.
14 J. Gao, X. Zhang, S. Xu, F. Tan, X. Li, Y. Zhang, Z. Qu, X. Quan and J. Liu, *Chem.-Eur. J.*, 2014, **20**, 1957-1963.
15 C. E. Hoyle and C. N. Bowman, *Angew. Chem., Int. Ed.*, 2010, **49**, 1540-1573.
16 D. Esquivel, O. van den Berg, F. J. Romero-Salguero, F. Du Prez and P. Van Der Voort, *Chem. Comm.*, 2013, **49**, 2344-2346.
17 O. Bortolini, L. Caciolli, A. Cavazzini, V. Costa, R. Greco, A. Massi and L. Pasti, *Green Chem.*, 2012, **14**, 992-1000.
18 Q. Chen, C. Xin, L.-L. Lou, K. Yu, F. Ding and S. Liu, *Catal. Lett.*, 2011, **141**, 1378-1383. View Article Online DOI: 10.1039/C6GC01494A
19 C. Baleizao, B. Gigante, H. Garcia and A. Corma, *J. Catal.*, 2003, **215**, 199-207.
20 J. Gehring, B. Trepka, N. Klinkenberg, H. Bronner, D. Schleheck and S. Polarz, *J. Am. Chem. Soc.*, 2016, **138**, 3076-3084.
21 A. K. Tucker-Schwartz, R. A. Farrell and R. L. Garrell, *J. Am. Chem. Soc.*, 2011, **133**, 11026-11029.
22 J. Gehring, D. Schleheck, B. Trepka and S. Polarz, *Appl. Mat. & Interf.*, 2015, **7**, 1021-1029.
23 C. Vercaemst, M. Ide, B. Allaert, N. Ledoux, F. Verpoort and P. Van Der Voort, *Chem. Comm.*, 2007, **22**, 2261-2263.
24 J. Ouwehand, J. Lauwaert, D. Esquivel, K. Hendrickx, V. Van Speybroeck, J. Thybaut, P. Van Der Voort, *Eur. J. Inorg. Chem.*, 2016, **13**, 2144-2151.
25 M. Ide, E. De Canck, I. Van Driessche, F. Lynen and P. Van der Voort, *RSC Adv.*, 2015, **5**, 5546-5552.
26 F. Goethals, B. Meeus, A. Verberckmoes, P. Van Der Voort and I. Van Driessche, *J. Mater. Chem.*, 2010, **20**, 1709-1716.
27 K. Landskron, B. D. Hatton, D. D. Perovic and G. A. Ozin, *Science*, 2003, **302**, 266-269.
28 K. Yamaguchi, K. Mori, T. Mizugaki, K. Ebitani and K. Kaneda, *J. Am. Chem. Soc.*, 2000, **122**, 7144-7145.
29 G. Csjernyik, A. H. Ell, L. Fadini, B. Pugin and J. E. Backvall, *J. Org. Chem.*, 2002, **67**, 1657-1662.
30 A. Dijksman, A. Marino-Gonzalez, A. M. I. Payeras, I. Arends and R. A. Sheldon, *J. Am. Chem. Soc.*, 2001, **123**, 6826-6833.
31 W. H. Fung, W. Y. Yu and C. M. Che, *J. Org. Chem.*, 1998, **63**, 2873-2877.
32 A. Hanyu, E. Takezawa, S. Sakaguchi and Y. Ishii, *Tetrahedron Lett.*, 1998, **39**, 5557-5560.
33 B. Karimi, D. Elhamifar, O. Yari, M. Khorasani, H. Vali, J. H. Clark and A. J. Hunt, *Chem.-Eur. J.*, 2012, **18**, 13520-13530.
34 I. E. Marko, P. R. Giles, M. Tsukazaki, I. Chelle-Regnaut, C. J. Urch and S. M. Brown, *J. Am. Chem. Soc.*, 1997, **119**, 12661-12662.
35 K. Yamaguchi and N. Mizuno, *Angew. Chem., Int. Ed.*, 2002, **41**, 4538-4541.
36 S. Ganesamoorthy, M. M. Tamizh, K. Shanmugasundaram and R. Karvembu, *Tetrahedron Lett.*, 2013, **54**, 7035-7039.
37 E. De Canck, I. Dosuna-Rodriguez, E. M. Gaigneaux and P. Van der Voort, *Materials*, 2013, **6**, 3556-3570.
38 T. Koiwa, Y. Masuda, J. Shono, Y. Kawamoto, Y. Hoshino, T. Hashimoto, K. Natarajan and K. Shimizu, *Inorg. Chem.*, 2004, **43**, 6215-6223.
39 M. J. Frisch, G. W. Trucks, H. B. Schlegel, G. E. Scuseria, M. A. Robb, J. R. Cheeseman, G. Scalmani, V. Barone, B. Mennucci, G. A. Petersson, H. Nakatsuji, M. Caricato, X. Li, H. P. Hratchian, A. F. Izmaylov, J. Bloino, G. Zheng, J. L. Sonnenberg, M. Hada, M. Ehara, K. Toyota, R. Fukuda, J. Hasegawa, M. Ishida, T. Nakajima, Y. Honda,

O. Kitao, H. Nakai, T. Vreven, J. A. Montgomery Jr., J. E. Peralta, F. Ogliaro, M. J. Bearpark, J. Heyd, E. N. Brothers, K. N. Kudin, V. N. Staroverov, R. Kobayashi, J. Normand, K. Raghavachari, A. P. Rendell, J. C. Burant, S. S. Iyengar, J. Tomasi, M. Cossi, N. Rega, N. J. Millam, M. Klene, J. E. Knox, J. B. Cross, V. Bakken, C. Adamo, J. Jaramillo, R. Gomperts, R. E. Stratmann, O. Yazyev, A. J. Austin, R. Cammi, C. Pomelli, J. W. Ochterski, R. L. Martin, K. Morokuma, V. G. Zakrzewski, G. A. Voth, P. Salvador, J. J. Dannenberg, S. Dapprich, A. D. Daniels, Ö. Farkas, J. B. Foresman, J. V. Ortiz, J. Cioslowski and D. J. Fox, Gaussian, Inc., Wallingford, CT, USA, 2009.

40 A. D. Becke, *J. Chem. Phys.*, 1993, **98**, 5648-5652.

41 C. Lee, W. Yang and R. G. Parr, *Phys. Rev. B*, 1988, **37**, 785-789.

42 N. C. Handy and A. J. Cohen, *Mol. Phys.*, 2001, **99**, 403-412.

43 W.-M. Hoe, A. J. Cohen and N. C. Handy, *Chem. Phys. Lett.*, 2001, **341**, 319-328.

44 J. Perdew, K. Burke and M. Ernzerhof, *Phys. Rev. Lett.*, 1997, **78,** 1396-1396.

45 J. P. Perdew, K. Burke and M. Ernzerhof, *Phys. Rev. Lett.*, 1996, **77**, 3865-3868.

46 F. Weigend, *Phys. Chem. Chem. Phys.*, 2006, **8**, 1057-1065.

47 F. Weigend and R. Ahlrichs, *Phys. Chem. Chem. Phys.*, 2005, **7**, 3297-3305.

48 S. Grimme, J. Antony, S. Ehrlich and H. Krieg, *The J. Chem. Phys.*, 2010, **132,** 154104.

49 S. Grimme, S. Ehrlich and L. Goerigk, *J. Comput. Chem.*, 2011, **32**, 1456-1465.

50 L. Goerigk and S. Grimme, *Phys. Chem. Chem. Phys.*, 2011, **13**, 6670-6688.

51 S. F. Boys and F. Bernardi, *Mol. Phys.*, 1970, **19**, 553-566.

52 A. Zuerner, J. Kirstein, M. Doeblinger, C. Braeuchle and T. Bein, *Nature*, 2007, **450**, 705-709.

53 T. Bogaerts, S. Wouters, P. Van der Voort and V. Van Speybroeck, *ChemCatChem*, 2015, **7**, 2711-2719.

54 M. Swart, A. W. Ehlers and W. Koop, *Mol. Phys.*, 2004, **102**, 2467-2474.

55 Y. Minenkov, Å. Singstad, G. Occhipinti and V. R. Jensen, *Dalton Trans.*, 2012, **41**, 5526-5541.

56 J. Zhang, Q. Jiang, D. Yang, X. Zhao, Y. Dong and R. Liu, *Chem. Sci.*, 2015, **6**, 4674-4680.

57 S. E. Davis, M. S. Ide and R. J. Davis, *Green Chem.*, 2013, **15**, 17-45.

58 Z. Shi, C. Zhang, C. Tang and N. Jiao, *Chem. Soc. Rev.*, 2012, **41**, 3381-3430.

59 W. Wang, J. E. Lofgreen, G. A. Ozin, *Small*, 2010, **23**, 2634-2642.

60 D. Esquivel, C. Jimenez-Sanchidrian an F. J. Romero-Salguero, *Mater. Lett*., 2011, **65**, 1460-1462.

61 C. M. Li, H. Yang, X. Shi, R. Liu and Q. H. Yang, *Microporous Mesoporous Mater.*, 2007, **98**, 220-226.

62 G. Morales, G. Athens, B. F. Chmelka, R. van Grieken and J. A. Melero, *J. Catal.*, 2008, **254**, 205-217.

63 A. Karam, J. C. Alonso, T. I. Gerganova, P. Ferreira, N. Blon, J. Barrault and F. Jerome, *Chem. Commun.*, 2009, 7000-7002.

View Article Online
DOI: 10.1039/C6GC01494A

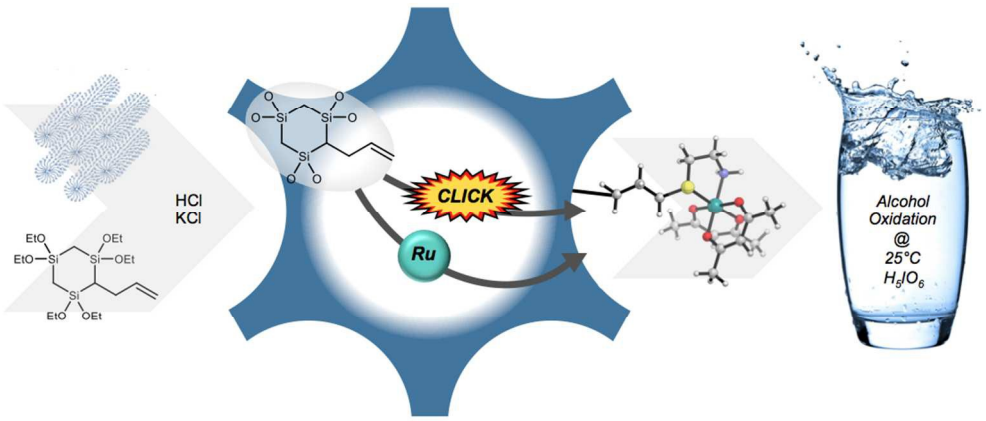

398x167mm (72 x 72 DPI)